

Segmentation of Magnetic Resonance Images of
the Knee using Three-dimensional
Active Shape Models

Klas Josephson

December 14, 2004

Abstract

In this thesis a fully automated segmentation system for the bones of the knee in Magnetic Resonance Images is presented. Several data sets were segmented manually. The resulting structures are first represented by unorganised point clouds. With level set methods surfaces were fitted to these point clouds. The iterated closest point algorithm was then applied to establish correspondences between different surfaces. Both surfaces and correspondences were used to build a three dimensional statistical shape model of the major bones in the knee. The resulting model is used to automatically segment the knee in subsequent data sets through a method called Active Shape Models. The result of the segmentation is promising, but the quality of the segmentation is dependent on the initial guess. The segmentation of the major bones is useful for establishing the position of other parts of the knee, for further segmentation, feature extraction and interpretation of the images. The algorithms have also been tested on SPECT images of the brain with even better results.

Acknowledgments

The author would like to thank the following persons for the supervision during the work with this thesis. Magnus Tägil at the Department of Orthopedics in Lund for the proposal of the thesis and for providing the images on which this thesis are based. I also would like to thank my supervisor and examiner Kalle Åström and my supervisors Anders Ericsson and Johan Karlsson at the Center for Mathematical Sciences, Lund Institute of Technology who have been very helpful in the daily work on this thesis.

Contents

1	Introduction	1
2	Background	3
2.1	Related Work	3
2.2	Active Shape Models	4
2.3	Image Acquisition	4
2.4	Related Ongoing Work	5
3	Shape Reconstruction	6
3.1	Building the Point Cloud	6
3.2	Calculating the Triangulation	6
3.3	Result on Real Data	9
4	Finding Corresponding Points	11
4.1	Iterative Closest Point	11
5	Aligning Training Set	13
6	Building the Shape Model	17
6.1	Principal Component Analysis	17
6.2	Making New Shapes From the Model	18
6.3	Shape Model of the Femur	19
7	Segmentation with Active Shape Models	21
7.1	Multi-Resolution Approach for Active Shape Models	21
7.2	Getting the Initial Guess	22
7.3	Finding Suitable Points	24
7.4	Updating Parameters	26
8	Experiments	27
8.1	Shape Reconstruction from Point Cloud	27
8.2	Finding Corresponding Points	27
8.3	Segmentation	28
9	Further Work	31
9.1	Improvements on the Model Building	31
9.2	Further Work on Segmentation	32
9.3	A New Approach for the Searching After New Points	32
9.4	Decision Support System	33

List of Figures

2.1	Explanation of the three slice directions.	4
2.2	Names of the bones in the knee.	5
3.1	Unorganised point cloud of the femur.	7
3.2	A point cloud generated from SPECT images of the brain.	9
3.3	The surface fitted to an unorganised point cloud of the femur. . .	10
3.4	The surface fitted to an unorganised point cloud of the brain. . .	10
5.1	Shape description	14
6.1	Random points where PCA is applied to find the main direction. The main directions are plotted with 2 std.	19
6.2	The first five shape modes of the femur.	20
7.1	Three levels of a Gaussian pyramid.	22
7.2	The 1-D spatial information of the 2-D images.	23
7.3	Search in normal direction	25
8.1	A good result from the segmentation when only plain edge de- tection have been used while updating landmark positions.	28
8.2	A bad result from the segmentation when only plain edge detec- tion have been used while updating landmarks positions.	29
8.3	Segmentation result when models of the gray level structure were used.	29
8.4	Segmentation result on the brain	30
9.1	An example of a profile that has two different forms of gray level signature.	32
9.2	A new approach for edge detection	33

Chapter 1

Introduction

Hospitals today produce numerous diagnostic images such as Magnetic Resonance Imaging (MRI), Single Photon Emission Computed Tomography (SPECT), Computed Tomography (CT) and digital mammography. These technologies have greatly increased the knowledge of diseases and they are a crucial tool in diagnosis and treatment planning.

The growing number of images and the increasing resolution of the images in the medical field have made it necessary to use computerised tools as a help to find anatomical structures and to make decision support systems.

Today almost all analysis of images is still done by manual inspection by the doctors even though the images are digitalised from the beginning. Even for an experienced doctor the diagnosis can be hard to state and it is often time consuming especially in three dimensional images.

The aim of this master thesis is to automatically segment the bones from MRIs of the knee for pre-surgery analysis. To do that a method called active shape is used. An Active Shape Model (ASM) uses the mean shape and the typical ways that object variate to segment it. To build the ASM methods for making surface reconstruction from point clouds and methods for finding corresponding points over the training sets have also been used.

The implementation of this thesis was made in C++ and Matlab. C++ was used for calculating corresponding points over the training set and for building the shape model. The C++ programs were based on the The Visualization Toolkit (VTK) which is an open source software system for 3D computer graphics (<http://www.vtk.org>). To improve the speed of the surface fitting the fast marching algorithm was implemented in C by Magnus Wendt. None of the algorithms are extremely time consuming and therefore it was not necessary to rewrite the Matlab part into C.

The author is studying toward a Master of Sciences in Engineering Physics with focus on image analysis and computer vision. This thesis was made in cooperation between the Center for Mathematical Science, Lund Institute of Technology and the Department of Orthopedics in Lund. The MR images were produced at several hospitals in southern Sweden.

This thesis starts in the next chapter with a background on MRI and a study of related work. In Chapter 3 the theory for the surface fitting algorithm is reviewed. Chapter 4 includes the method for finding corresponding points over the training set and Chapter 5 describes how to align those points. In

Chapter 6 the method for building the shape model is presented. Chapter 7 holds the algorithms used to segment objects with the aid of the shape model. Later in Chapter 8 the result of the work is showed and discussed and suggestions for further work are presented in Chapter 9.

Chapter 2

Background

2.1 Related Work

For segmentation of medical images many different methods have been used. Pham et al. [11] make a review of a number of approaches.

The most commonly used of those approaches are Thresholding and Region Growing. These are easy to implement and produces good results in many cases. Thresholding works by creating a binary partitioning of the image intensities. The threshold value are predefined or in some way calculated and the pixels with values on either side of the threshold value are divided into different groups.

In region growing a seed point is decided and all connected points that fulfils a predefined criteria are then labeled as the same group. After that all points connected to the points labeled in the previous step are checked. If these also fulfils the criteria they are labeled in the same group. This algorithm continues until no more connected pixels fulfils the criteria.

2.1.1 Segmentation of MR Images of the Knee

Earlier work on segmentation is mainly concentrated on distinguishing cartilage from the other parts of the knee. Many different methods have been used to do that, but most of these are not fully automatic and therefore needs an expert either to initialise the process or to check and fix the result. One way that has been used is region growing [16] but on knees the result was not good due to the lack of contrast between bone tissue and fat.

A common method for the segmentation is to fit B-splines curves to the edges in two dimensional slices [4], [5]. The edges were in these articles located by the user. In [14] B-splines are also the choice but in this case the operator only had to initiate the edge in one slice and after that a snake improved the segmentation in the slice. For the other slices the result from the slice next to it was chosen as a start guess of the outline. The so called watershed method is applied in [8] but the result was not good. But in [9] a modified version of the watershed algorithm is used with good result but still it needs some assistance from the operator.

2.2 Active Shape Models

In this thesis Active Shape Models [6] is the choice for the segmentation. This method uses a technique with a statistical model of the shape of the object to be analysed. The model is constructed from a training set where the object has been segmented in another way (in most cases manually).

An active shape model represents the shapes with the mean shape and a linear combination of variation modes. This can be written in matrix form as

$$\mathbf{x} = \bar{\mathbf{x}} + \Phi \mathbf{b}, \quad (2.1)$$

where \mathbf{x} is the new shape, $\bar{\mathbf{x}}$ the mean shape, Φ the variation modes and \mathbf{b} the parameters to the variation modes. If the model is well suited to the object that is to be segmented the model should be able to represent the new shape and the parameters in the \mathbf{b} vector should be relatively small.

Active shape have been used by Cootes et al. in [6]. There they only worked in two dimensions on the cartilage of the knee. In this thesis a three dimensional approach of the active shape is applied to segment out the whole structure in all image slices at once.

2.3 Image Acquisition

MRI in medicine was developed in the 80's by Sir Peter Mansfield and Paul C. Lauterbur and they were awarded the The Nobel Prize in Physiology or Medicine in 2003. The technique uses the nuclear spin of the hydrogen atoms. With a strong magnetic field (about 1–10 T) more hydrogen atoms have their spin pointed as the magnetic field than in the opposite direction. This makes it possible to pump the hydrogen atoms with radio-photons (about 100 MHz) and then there will be resonance in the hydrogens atoms and a radio frequency can be collected to measure the structure inside the body. For more information about MRI see [15].

The images are produced in slices, these slices are taken in three different directions, sagittal, coronal and transversal. In Figure 2.1 the three different views are shown.

The major bones in the knee are referred to as femur and tibia. Figure 2.2 shows the name of the bones.



Figure 2.1: The three slice direction of medical images. To the left a sagittal view, in the middle coronal view and to the right transversal view.

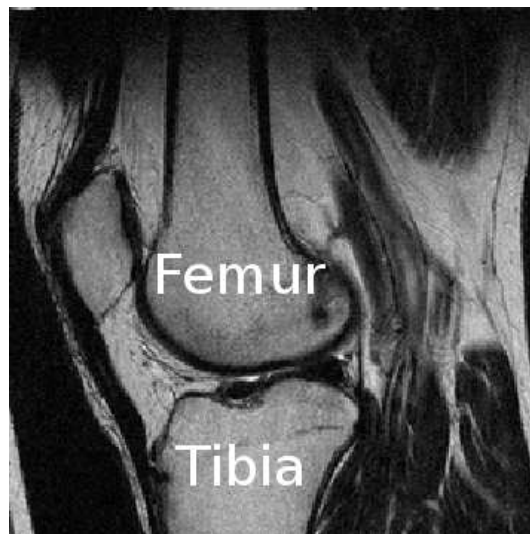


Figure 2.2: Names of the bones in the knee.

Medical images used in this thesis are stored in the DICOM format [2]. In the DICOM standard the directions of the axes are fully defined by the patient's orientation. The x -axis is increasing to the left hand side, the y -axis increases towards the back of the patient and the z -axis increases towards the head of the patient. These definition makes the coordinate system right handed. In the rest of the report these definitions are used when medical images are discussed.

2.4 Related Ongoing Work

Parallel to this thesis another master thesis has been started at the Center for Mathematical Science. That thesis works with segmentation of the brain in SPECT images. Because of that all algorithms made in this thesis have also been tested on SPECT images of the brain.

Chapter 3

Shape Reconstruction from Point Clouds

From an unorganised point cloud the aim is to get a triangulation of the surface that the points are located at. To do that first of all the point cloud of the femur has to be constructed. After that a level set approach is used for the surface fitting.

3.1 Building the Point Cloud

The point cloud is built from points marked manually in the MR slices. The marking is done in every slice. The points marked are connected with cubic splines and therefore it is more points than those which are marked that are saved, this gives a denser point cloud. During the marking the splines are visible and the result can be visual examined.

To every image slice an information tag is connected. This tag contains information which makes it possible to locate every image pixel in a 3D-space. The coordinate system is the same for the slices in different directions and thus different slice directions can be mixed together. An example of a point cloud can be seen in Figure 3.1.

3.2 Calculating the Triangulation

There are several methods to find the surface to an unorganised point cloud. The easiest way to do this is to start with one point, then find the two points which are closest and number that group as the first triangle. After that always chose the closest not used point to the line connecting two points and a new triangle will be made. Do this for all points and the triangulation is completed.

The problem with this approach is that the femur is marked in the MR slices. Samples are taken from sagittal, coronal and sometimes transversal slices and are then mixed together. This makes a noisy point cloud as in Figure 3.1. To handle the noisy data a level set approach is used to reconstruct the surface. In [18] Zhao et al. developed a method which reconstructs a surface that is minimal to the distance transform to the data set. This approach has problem when the



Figure 3.1: Unorganised point cloud of the femur.

point clouds are noisy. Later Shi and Karl [12] proposed a data-driven, Partial Differential equation (PDE) based, level set method that handles noisy data.

The idea of the level set method is to represent the surface as an implicit distance function which is zero at the surface and negative inside. The function is then updated to solve a PDE that is constructed in such a way that it will have a minimum at the true surface. By updating the function iteratively it will fit to the surface. The problem is formulated as follows:

Denote the points in the point cloud $\mathbf{X} = (\mathbf{x}_1, \dots, \mathbf{x}_n)$. And the distance function ϕ where $\phi = 0$ is the surface. With aid of the distance function the signed distance from a point to the surface, denoted as $g(\mathbf{x}_i, \phi)$, can be written

$$g(\mathbf{x}_i, \phi) = \phi(\mathbf{x}_i) = \int \phi(\mathbf{x}) \delta(\mathbf{x} - \mathbf{x}_i) dx, \quad (3.1)$$

where δ is the delta distribution. The distances are then collected in a vector $\mathbf{g}(\mathbf{X}, \phi)$. The problem can now be rewritten as an energy minimisation problem. The energy is then

$$E(\phi) = \underbrace{-\log p(\mathbf{g}(\mathbf{X}, \phi)|\phi)}_{E_d} + \mu \underbrace{\int \delta(\phi) |\nabla \phi| dx}_{E_s}, \quad (3.2)$$

where $p(\mathbf{g}(\mathbf{X}, \phi)|\phi)$ is the probability that the points \mathbf{X} has the shape ϕ . Here it is assumed that $p(\mathbf{g}(\mathbf{X}, \phi)|\phi)$ is a Gaussian distributed:

$$p(\mathbf{g}(\mathbf{X}, \phi)|\phi) \propto e^{-(\mathbf{g}-\mathbf{u})^T \mathbf{W}^{-1} (\mathbf{g}-\mathbf{u})/2}, \quad (3.3)$$

where \mathbf{u} is the mean distance and \mathbf{W} is the covariance matrix.

The distance function ϕ also has to fulfil the constraint $|\nabla \phi| = 1$ to ensure that it is a signed distance function. The E_d term describes how well the surface are suited to the points and the E_s term is for smoothing.

In each iteration of the surface reconstruction a step is taken in the steepest decent direction of the gradient. For the E_d the gradient is obtained as:

$$\frac{dE_d}{d\phi} = \frac{dE_d^T}{d\mathbf{g}} \frac{d\mathbf{g}}{d\phi}. \quad (3.4)$$

From (3.2) we have

$$\frac{dE_d}{d\mathbf{g}} = -\frac{1}{p} \frac{dp}{d\mathbf{g}}$$

and

$$\frac{d\mathbf{g}}{d\phi} = [\delta(\mathbf{x} - \mathbf{x}_1), \dots, \delta(\mathbf{x} - \mathbf{x}_n)]^T.$$

Now approximate $\delta(\mathbf{x})$ with

$$\delta_\alpha(\mathbf{x}) = \begin{cases} 0, & |\mathbf{x}| > \alpha, \\ \frac{1}{2\alpha} \left[1 + \cos\left(\frac{\pi|\mathbf{x}|}{\alpha}\right) \right], & |\mathbf{x}| < \alpha, \end{cases} \quad (3.5)$$

where $\alpha \geq 0$. Finally put the evolution step due to the negative gradient direction so that the step due to the E_d term is

$$\left[\frac{d\phi}{dt} \Big|_{\mathbf{x}=\mathbf{x}_0} \right]_d = - \sum_{i=1}^n \frac{dE_d}{dg(\mathbf{x}_i, \phi)} \delta_\alpha(\mathbf{x}_0 - \mathbf{x}_i). \quad (3.6)$$

To construct the component of the evolution speed for the function ϕ due to the data term over the whole domain, denoted as F_d , so that ϕ will remain a signed distance function, the method from [1] is followed, thus solving of the PDE:

$$\nabla\phi \cdot \nabla F_d = 0 \quad (3.7)$$

with the boundary condition

$$F_d(\mathbf{x}_0) = \left[\frac{d\phi}{dt} \Big|_{\mathbf{x}=\mathbf{x}_0} \right]_d \quad (3.8)$$

obtained from (3.6) is made. This PDE is derived so that $|\nabla\phi| = 1$ will remain true. The smooth terms evolution speed is as Zhao et al. showed in [19]

$$\left[\frac{d\phi}{dt} \right]_s = \left(\nabla \cdot \frac{\nabla\phi}{|\nabla\phi|} \right) |\nabla\phi|. \quad (3.9)$$

Combining the two terms of energy gives the final evolution speed as

$$\frac{d\phi}{dt} = F_d |\nabla\phi| + \mu \left(\nabla \cdot \frac{\nabla\phi}{|\nabla\phi|} \right) |\nabla\phi|. \quad (3.10)$$

Here μ is used to make a good balance between the surface fitting and the smoothing.

The use of the approximated delta distribution makes the method robust to local minima, because a point only effects the surface close to the point. Thus it is possible to make an initial guess close to the real surface which reduce the time for the algorithm significant. The α parameter in (3.5) can be varied to make the surface fitting algorithm able to handle data sets with different sparsity.

Between every step of the iteration the fast marching algorithm is used to update the distance function, this is necessary to keep $|\nabla\phi| = 1$. For more about the fast marching algorithm see Adalsteinsson and Sethian in [1].

The initial guess is obtained by making a function that in every point has the value of the positive distance to the nearest point in the point cloud. After that those points that are close to the surface are set to zero. This makes the function divided into two parts divided by a band where the function is zero. A new distance function is now made that measures the distance to the outer edge of the zero area, this is a signed distance function which is negative inside the surface. Finally the surface are moved by the half length of the thickness of the zero band. The moving of the surface is done by subtracting the distance of the movement to the whole volume. This makes an approximated surface that is very good at convex parts of the surface but not that good in the concave parts.

3.3 Result on Real Data

The surface reconstruction has problems when the data is not dense enough. In the femur example in Figure 3.1 that does not produce any problems. The result can be seen in Figure 3.3. But in the SPECT images the used data was less dense and it was necessary to interpolate more points to get a good surface. An image of the point cloud in the SPECT images can be seen in Figure 3.2 and the result of the surface fitting when more points were interpolated can be seen in Figure 3.4.

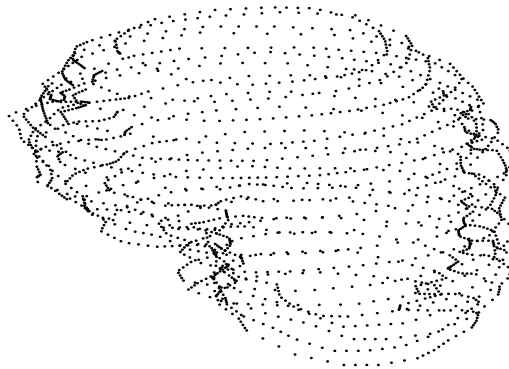


Figure 3.2: A point cloud generated from SPECT images of the brain.

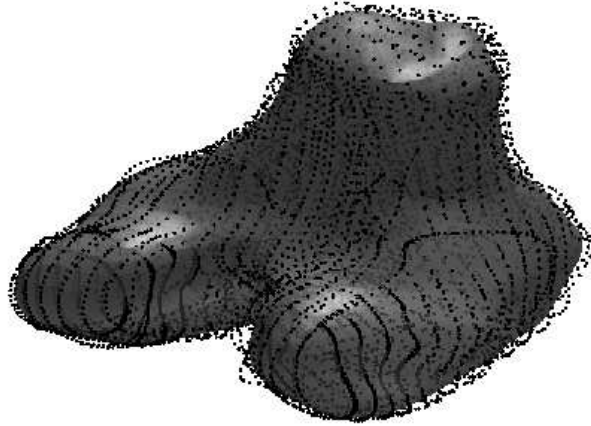


Figure 3.3: The surface fitted to an unorganised point cloud. Even though the surface is a little bit transparent it is hard to see the points inside the femur, this makes the surface look like it lies inside the points.

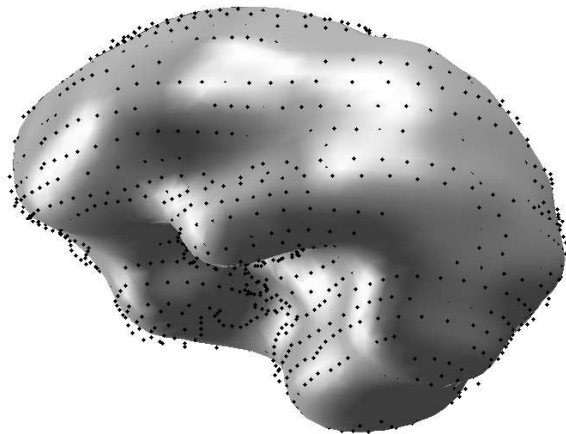


Figure 3.4: The result of the surface fitting when the points represent the brain from SPECT images.

Chapter 4

Finding Corresponding Points

In shape modelling it is of great importance that during the training a dense correspondence is established over the training set. This part is the most difficult and the most important for a good result of the upcoming segmentation. The correspondence is normally established by placing landmarks at the surface.

A landmark is a point on the surface. These are labeled, thereby giving correspondence between points on the surfaces in the training set. A good choice of landmarks in a medical image describes something that are of anatomical interest, for example a good landmark can be the tip of the index finger. Usually these points are not many enough. It is also hard to find these automatically and to mark them manually is very time consuming and error prone.

An approach to find correspondence between shapes is to have corresponding parametrisation of the shapes. If the shapes later are sampled according to the parametrisation it is possible to find corresponding points of two shapes. In the remaining part of this thesis these points are referred to as landmarks.

4.1 Iterative Closest Point

In this thesis the correspondence of points over the training set is established by the Iterative Closest Point (ICP) algorithm [3]. With the ICP algorithm a corresponding triangulation of the surface for the bones is achieved over the training set. The problem is to calculate new vertices on the surface while the shape remains the same.

The ICP algorithm matches two overlapping surfaces. It uses one as source surface and one as target. The triangulation of the source is kept and the aim is to get an optimal corresponding triangulation on the target surface. To do this an iterative process is applied with the steps as follows:

1. For each vertex at the source surface find the closest point at the target surface.
2. Compute the transformations from the source to the new points, located in the previous step, that minimise the mean square error between the two point clouds with translation and rotation.

3. Apply the transformation
4. Return to 1 until the improvement between two iterations is less than a threshold value $\tau > 0$.

When the threshold value is reached the closet points on the target surface are calculated one last time and these points gives the new vertices on the target surface.

This algorithm gives two surfaces with corresponding triangulation and each point can be looked at as a landmark with corresponding landmark at the other surface. If the same source surface is always used and the target surface is switched it is possible to find corresponding landmarks in a larger training set.

Chapter 5

Aligning the Training Set Using Procrustes Analysis

When the corresponding landmarks are found the next step is to align the landmarks under similarity transformations. This is done because only the shape should be considered in the shape model and the translation, scale and rotation should be filtered out.

Even if shape is a common expression in the every day language it is good to have a more mathematical definition of it. An intuitive one is as follows:

Definition 5.1 (shape) *Two geometric objects have the same shape, if one can be mapped onto the other by a similarity transformation.*

Similarity transformations only effects translations, rotation and scaling. This definition does not allow flipping when shapes are compared. (See Figure 5.1.)

The most popular way to make the aligning is the Procrustes Analysis [7]. With this method the aim is to align one shape \mathbf{X} ,

$$\mathbf{X} = (\mathbf{x}_1, \dots, \mathbf{x}_n) = \begin{pmatrix} x_{11} & \dots & x_{1n} \\ \vdots & \ddots & \vdots \\ x_{m1} & \dots & x_{mn} \end{pmatrix}, \quad (5.1)$$

where m is the dimension and n the number of points, with another shape \mathbf{Y} with corresponding landmarks. This is done by minimising

$$\|\mathbf{X} - T(\mathbf{Y})\|^2$$

over T , where T is a similarity transform.

Alignment of two shapes, $\mathbf{X} = (\mathbf{x}_1, \dots, \mathbf{x}_n)$ and $\mathbf{Y} = (\mathbf{y}_1, \dots, \mathbf{y}_n)$, in three dimensions can be calculated explicitly. Umeyama presents a way to do this [17]. The method finds the minimum of the mean squared error $e^2(\mathbf{R}, \mathbf{t}, c)$ of two point patterns,

$$e^2(\mathbf{R}, \mathbf{t}, c) = \frac{1}{n} \sum_{i=1}^n \|\mathbf{y}_i - (c\mathbf{R}\mathbf{x}_i + \mathbf{t})\|^2, \quad (5.2)$$

with respect to rotation \mathbf{R} , scale factor c and translation \mathbf{t} . The dimensionality are usually two or as in this case three. Before the theorem is showed a lemma is presented.

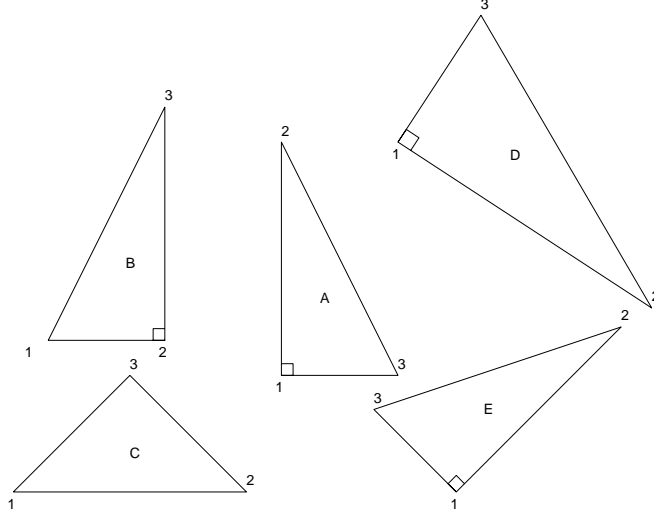


Figure 5.1: Triangle D and E have the same shape. On triangle B the labels can be moved and it will then have the same shape as D and E. Triangle A is flipped compared to D and E and therefore does not have the same shape. Triangle C has a different shape compared to the other triangles.

Lemma 5.1 *Let \mathbf{A} and \mathbf{B} be $m \times n$ matrices, and \mathbf{R} an $m \times m$ rotation matrix, and $\mathbf{U}\mathbf{\Sigma}\mathbf{V}^T$ a singular value decomposition of $\mathbf{A}\mathbf{B}^T$ ($\mathbf{U}\mathbf{U}^T = \mathbf{V}\mathbf{V}^T = \mathbf{I}$, $\mathbf{\Sigma} = \text{diag}(\sigma_i)$, $\sigma_1 \geq \sigma_2 \geq \dots \geq \sigma_m \geq 0$). Then the minimum value of $\|\mathbf{A} - \mathbf{R}\mathbf{B}\|^2$ with respect to \mathbf{R} is*

$$\min_{\mathbf{R}} \|\mathbf{A} - \mathbf{R}\mathbf{B}\|^2 = \|\mathbf{A}\|^2 + \|\mathbf{B}\|^2 - 2\text{tr}(\mathbf{\Sigma}\mathbf{S}), \quad (5.3)$$

where

$$\mathbf{S} = \begin{cases} \mathbf{I} & \text{if } \det(\mathbf{A}\mathbf{B}^T) \geq 0, \\ \text{diag}(1, 1, \dots, 1, -1) & \text{if } \det(\mathbf{A}\mathbf{B}^T) < 0. \end{cases} \quad (5.4)$$

When $\text{rank}(\mathbf{A}\mathbf{B}^T) \geq m - 1$, the optimum rotation matrix \mathbf{R} which achieves the above minimum value is uniquely determined and given by

$$\mathbf{R} = \mathbf{U}\mathbf{S}\mathbf{V}^T, \quad (5.5)$$

where \mathbf{S} in (5.5) must be chosen as

$$\mathbf{S} = \begin{cases} \mathbf{I} & \text{if } \det(\mathbf{U}) \det(\mathbf{V}) = 1, \\ \text{diag}(1, 1, \dots, 1, -1) & \text{if } \det(\mathbf{U}) \det(\mathbf{V}) = -1. \end{cases} \quad (5.6)$$

when $\det(\mathbf{A}\mathbf{B}^T) = 0$ ($\text{rank}(\mathbf{A}\mathbf{B}^T) = m - 1$).

The proof of the lemma can be found in [17]. There the following theorem is also proved using the lemma.

Theorem 5.1 Let $\mathbf{X} = (\mathbf{x}_1, \dots, \mathbf{x}_n)$ and $\mathbf{Y} = (\mathbf{y}_1, \dots, \mathbf{y}_n)$ be corresponding points patterns in m -dimensional space. The minimum value ε^2 of the mean square error

$$e^2(\mathbf{R}, \mathbf{t}, c) = \frac{1}{n} \sum_{i=1}^n \|\mathbf{y}_i - (c\mathbf{R}\mathbf{x}_i + \mathbf{t})\|^2 \quad (5.7)$$

of these point sets with respect to the similarity transformation is given by

$$\varepsilon^2 = \sigma_y^2 - \frac{\text{tr}(\boldsymbol{\Sigma}\mathbf{S})^2}{\sigma_x^2}, \quad (5.8)$$

where

$$\bar{\mathbf{x}} = \frac{1}{n} \sum_{i=1}^n \mathbf{x}_i, \quad (5.9)$$

$$\bar{\mathbf{y}} = \frac{1}{n} \sum_{i=1}^n \mathbf{y}_i, \quad (5.10)$$

$$\sigma_x^2 = \frac{1}{n} \sum_{i=1}^n \|\mathbf{x}_i - \bar{\mathbf{x}}\|^2, \quad (5.11)$$

$$\sigma_y^2 = \frac{1}{n} \sum_{i=1}^n \|\mathbf{y}_i - \bar{\mathbf{y}}\|^2, \quad (5.12)$$

$$\mathbf{C}_{xy} = \frac{1}{n} \sum_{i=1}^n (\mathbf{y}_i - \bar{\mathbf{y}})(\mathbf{x}_i - \bar{\mathbf{x}})^T, \quad (5.13)$$

and let a singular value decomposition of \mathbf{C}_{xy} be $\mathbf{U}\boldsymbol{\Sigma}\mathbf{V}^T$ ($\boldsymbol{\Sigma} = \text{diag}(\sigma_i)$, $\sigma_1 \geq \sigma_2 \geq \dots \geq \sigma_n \geq 0$), and

$$\mathbf{S} = \begin{cases} \mathbf{I} & \text{if } \det(\mathbf{C}_{xy}) \geq 0, \\ \text{diag}(1, 1, \dots, 1, -1) & \text{if } \det(\mathbf{C}_{xy}) < 0, \end{cases} \quad (5.14)$$

\mathbf{C}_{xy} is a covariance matrix of \mathbf{X} and \mathbf{Y} , $\bar{\mathbf{x}}$ and $\bar{\mathbf{y}}$ are mean vectors of \mathbf{X} and \mathbf{Y} , and σ_x and σ_y are variance around the mean vectors of \mathbf{X} and \mathbf{Y} , respectively.

When $\text{rank}(\mathbf{C}_{xy}) \geq m-1$, the optimum transform parameters are determined uniquely as follows:

$$\mathbf{R} = \mathbf{U}\mathbf{S}\mathbf{V}^T, \quad (5.15)$$

$$\mathbf{t} = \bar{\mathbf{y}} - c\mathbf{R}\bar{\mathbf{x}}, \quad (5.16)$$

$$c = \frac{1}{\sigma_x^2} \text{tr}(\boldsymbol{\Sigma}\mathbf{S}), \quad (5.17)$$

$$(5.18)$$

where \mathbf{S} in (5.15) must be chosen as

$$\mathbf{S} = \begin{cases} \mathbf{I} & \text{if } \det(\mathbf{U}) \det(\mathbf{V}) = 1, \\ \text{diag}(1, 1, \dots, 1, -1) & \text{if } \det(\mathbf{U}) \det(\mathbf{V}) = -1, \end{cases} \quad (5.19)$$

when $(\text{rank}(\mathbf{C}_{xy}) = m-1)$.

The theorem gives a way to align two data sets \mathbf{X} and \mathbf{Y} as close as possible under similarity transform. But in this thesis not only two data sets but the whole training set is to be aligned. Therefore an iterative approach has been used. The steps are as follows [6]:

1. Translate the examples so that their center of mass are in origin.
2. Chose one example as initial guess of the mean shape, $\bar{\mathbf{x}}$, and scale it so that $\|\bar{\mathbf{x}}\| = 1$.
3. Record the first estimate as $\bar{\mathbf{x}}_0$ to define the default reference frame.
4. Align all the shapes to the estimated mean shape. Do this as in theorem 5.1.
5. Estimate a new mean shape $\bar{\mathbf{x}}$.
6. Constrain the new mean shape by aligning it with $\bar{\mathbf{x}}_0$ and scale it so $\|\bar{\mathbf{x}}\| = 1$.
7. Return to 4 until convergence.

When the corresponding points are aligned it is possible to move forward and calculate a shape model of the knee.

Chapter 6

Building the Shape Model

In this part is described how a shape model is built and what the benefits are. The shape of an object is described by n points. In this thesis the points are in three dimensional space but it could also be higher or lower dimension with for example the time dimension as an extra dimension.

6.1 Principal Component Analysis

With n landmarks, $\mathbf{X}_i = (\mathbf{x}_1, \dots, \mathbf{x}_n)^T$ where \mathbf{x}_i are m -dimensional points, at the surface. The segmentation problem is nm dimensional. It is therefore of great interest to reduce the dimension and in an accurate way be able to decide whether a new shape is reasonable.

The aim is to find a model so that new shapes can be expressed by the linear model $\mathbf{x} = \bar{\mathbf{x}} + \Phi \mathbf{b}$, where \mathbf{b} is a vector of parameters for the shape modes. With this approach it is possible to constrain the parameters in \mathbf{b} so the new shape always will be reasonable.

To generate the model Φ from N training shapes, Principal Component Analysis (PCA) is applied. The landmarks \mathbf{X}_i used in the PCA are column stacked. In a three-dimensional case this can be written,

$$\tilde{\mathbf{x}}_i = [x_1, \dots, x_n, y_1, \dots, y_n, z_1, \dots, z_n]^T. \quad (6.1)$$

The approach to perform the PCA is as follows:

1. Compute the mean of the data

$$\bar{\mathbf{x}} = \frac{1}{N} \sum_{i=1}^N \tilde{\mathbf{x}}_i. \quad (6.2)$$

2. Construct the covariance matrix of the data

$$\mathbf{C} = \frac{1}{N-1} \sum_{i=1}^N (\tilde{\mathbf{x}}_i - \bar{\mathbf{x}})(\tilde{\mathbf{x}}_i - \bar{\mathbf{x}})^T. \quad (6.3)$$

3. Compute the eigenvectors, Φ_i and the corresponding eigenvalues σ_i of \mathbf{C} .

The matrix \mathbf{C} has the size $nm \times nm$ and it can be very time consuming to calculate the eigenvectors of the \mathbf{C} matrix (in this case \mathbf{C} has the size of about 12000×12000). But if the number of training examples is fewer than the number of landmarks times the dimension it is possible speed up the calculations. It will only be necessary to calculate eigenvalues and eigenvectors to an $N \times N$ matrix where N is the number of training examples. To show this approach the Singular Value Decomposition (SVD) [13] is used.

Let $\mathbf{X} = (\tilde{\mathbf{x}}_1 - \bar{\mathbf{x}}, \dots, \tilde{\mathbf{x}}_N - \bar{\mathbf{x}})$. Then \mathbf{X} can be decomposed by

$$\mathbf{X} = \mathbf{U}\mathbf{\Sigma}\mathbf{V}^T, \quad (6.4)$$

where \mathbf{U} is an $nm \times nm$ orthogonal matrix and \mathbf{V} is an $N \times N$ orthogonal matrix and $\mathbf{\Sigma}$ a diagonal matrix. For the PCA the eigenvectors to the covariance matrix $\mathbf{X}\mathbf{X}^T$ are of interest. These are the columns in \mathbf{U} in the expression

$$\mathbf{X}\mathbf{X}^T = (\mathbf{U}\mathbf{\Sigma}\mathbf{V}^T)(\mathbf{U}\mathbf{\Sigma}\mathbf{V}^T)^T = \mathbf{U}\mathbf{\Sigma}^2\mathbf{U}^T. \quad (6.5)$$

For the matrix $\mathbf{X}^T\mathbf{X}$ the SVD is

$$\mathbf{X}^T\mathbf{X} = (\mathbf{U}\mathbf{\Sigma}\mathbf{V}^T)^T(\mathbf{U}\mathbf{\Sigma}\mathbf{V}^T) = \mathbf{V}\mathbf{\Sigma}^2\mathbf{V}^T. \quad (6.6)$$

Now if the singular value σ_i is not zero the i :th column of the \mathbf{U} matrix can be calculated as

$$\mathbf{U}_i = \mathbf{X}\mathbf{V}\mathbf{e}_i/\sigma_i \quad (6.7)$$

where \mathbf{e}_i is the identity vector in direction i .

To compute the PCA in this way generates a faster algorithm if the number of examples in the training set are less then the number of landmarks times the dimension. The information that is lost are the rest of the eigenvectors with eigenvalues equal to zero, but those are of no interest in the shape model.

The eigenvalues of $\mathbf{X}^T\mathbf{X}$ are as showed in (6.5) and (6.6) the same as those for $\mathbf{X}\mathbf{X}^T$. The eigenvalues in $\mathbf{\Sigma}$ are sorted so $\sigma_1 \geq \sigma_2 \geq \dots \geq \sigma_n \geq 0$. The eigenvalues σ_i can be interpreted as the variance of the landmarks in the direction of the corresponding eigenvector \mathbf{U}_i , which describes a shape variation mode. This makes it possible to just use the big variation modes in the shape and not consider the small ones.

6.1.1 A PCA Example in Two Dimensions

If there is a set of points in the plane, the PCA describes the main direction of the points and the orthogonal vector. This makes it easy to find the direction of most variation. Figure 6.1 is an example where random points with different standard deviation (std) in x - and y -direction are rotated. The two principal components are plotted with 2 std in each direction.

6.2 Making New Shapes From the Model

From the model new shapes can be constructed. Let $\mathbf{\Phi} = [\mathbf{\Phi}_1, \dots, \mathbf{\Phi}_N]$, where $\mathbf{\Phi}_i$ are the columns in \mathbf{U} , i.e. the eigenvectors of the covariance matrix. It is not necessary to choose all the columns in \mathbf{U} , but if not all are used those

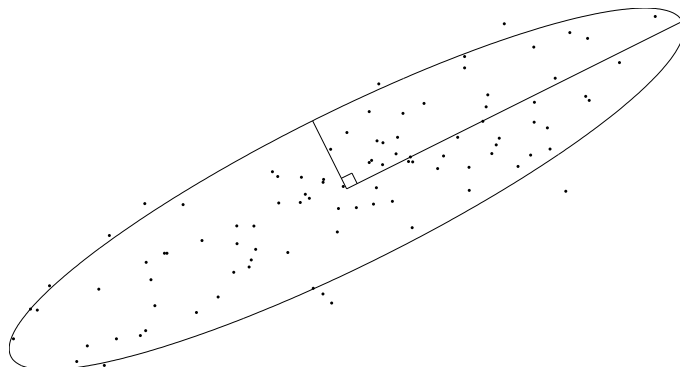


Figure 6.1: Random points where PCA is applied to find the main direction. The main directions are plotted with 2 std.

corresponding to the largest eigenvalues are to be chosen. The eigenvectors are called modes of variation or *shape modes*. New shapes can now be calculated as

$$\tilde{\mathbf{x}} = \bar{\mathbf{x}} + \Phi \mathbf{b} = \bar{\mathbf{x}} + \sum_{i=1}^N \Phi_i b_i. \quad (6.8)$$

Cootes et al. propose in [6] a constraint of the b_i parameters of $\pm 3\lambda_i$, where λ_i is the square root of the eigenvalues of the covariance matrix σ_i , to ensure that any new shape is similar to the shapes in the training set. This method is used in this thesis. Another way to constrain the parameters in the shape model would be to look at the probability that the new shape is from the training set and constrain the whole shape into a reasonable interval.

The numbers of shape modes to be used in the shape reconstruction can be limited and then chosen to represent a proportion of the variation in the training set. The proportion of variation that t eigenvectors cover are given by

$$V_t = \frac{\sum_{i=1}^t \sigma_i}{\sum \sigma_i}. \quad (6.9)$$

6.3 Shape Model of the Femur

From the aligned training set PCA is applied on the landmarks. The result can be seen in Figure 6.2. Where the first five shape modes are plotted with the mean shape in the middle. Over 50 % of the variation lies in the first shape mode. But that is because the MR images do not always covers exactly the same section of the knee.

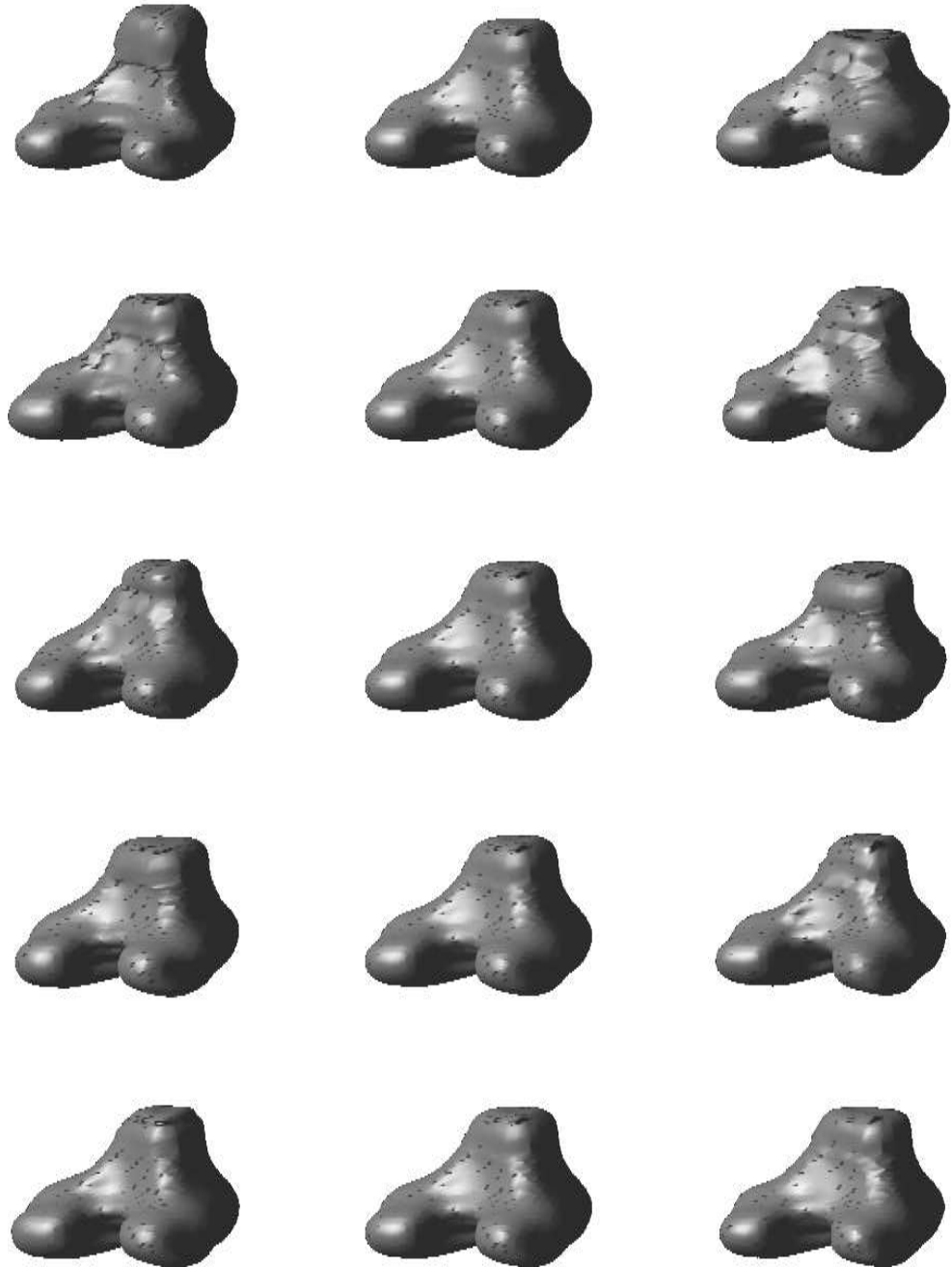


Figure 6.2: The first five shape modes of the femur. In the middle is the mean shape, to the left two std of the shape mode is subtracted and to the right they are added. Notice how most of the variation is in the first shape modes.

Chapter 7

Segmentation with Active Shape Models

The segmentation with active shape models is based on an iterative approach. After an initial guess the four steps below are iterated.

1. Search in the direction of the normal from every landmark to find a suitable point to place the landmark in.
2. Update the parameters for translation, rotation, scale and shape modes to make the best fit to the new points.
3. Apply constraints on the parameters.
4. Repeat until convergence.

7.1 Multi-Resolution Approach for Active Shape Models

To improve the robustness and the speed of the algorithm a multi-resolution approach is used. The idea of multi-resolution is to first search in a coarser image and then change to a more high resolution image when the search in the first image is not expected to improve. This improves the robustness because the amount of noise is less in the coarse level and therefore it is easier to find a way to the right object. The high resolution images are then used to find small structures. The speed accelerates because there is less data to handle in the coarse levels.

In the knee MR-images the voxels in the first level are ten times larger in the direction orthogonal to the slices than in the other directions. Because of that smoothing is made in every slice separately. Some of the images has a size of 512×512 pixels and others 256×256 , therefore those images with high resolution are smoothed down to 256×256 and that is considered as the first level. Then the levels are evaluated with smoothing in the slices in two steps which gives the coarsest level a resolution of 64×64 . There are usually between 20 and 25 slices in an image set. In Figure 7.1 a Gaussian pyramid with the three first levels can be seen.

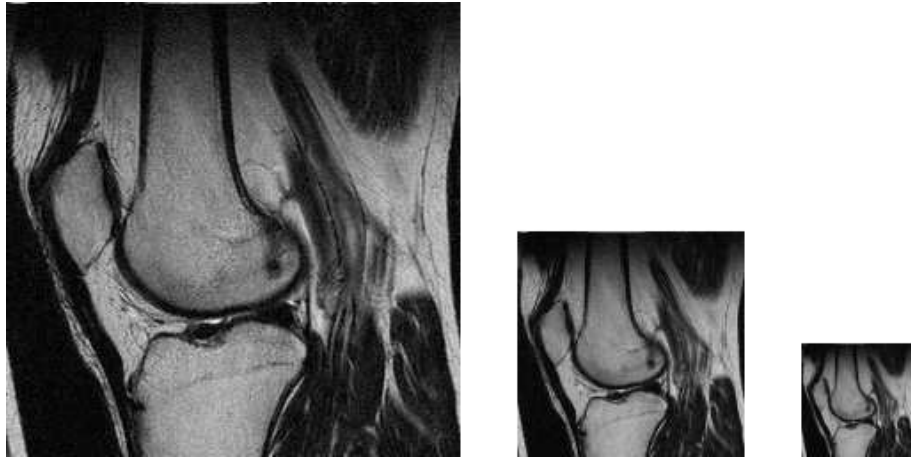


Figure 7.1: Three levels of the Gaussian pyramid. To the left the original image in the middle level 1 and to the right level 2, The size of the images are from left to right, 256×256 , 128×128 and 64×64 pixels.

7.2 Getting the Initial Guess

In order to obtain a fast and robust segmentation it is important to have a good initial estimation of the position and orientation. In the initial guess the shape is assumed to have the mean shape. This makes it necessary to find values of seven parameters to make a suitable initial guess in three dimensions (three for translation, one for scale and three for the rotation).

The first thing is to detect the lower part of the femur. To do that the 1-D spatial signature of a 2-D image is calculated by summarising the rows of the middle slice in the coarsest level. There will be a significant dip near the middle of the image which indicates the area between the femur and the tibia as seen in Figure 7.2. That row is set to the minimum z -coordinate of the shape and the top z -coordinate is set to the top of the slice. That result gives the translation in z -direction and the scale.

When the bottom z -coordinate is decided a transversal slice is taken a given distance above that location of the bottom z -coordinate. On this height the femur is usually located in the same area of the slice and a black line emerges around the bone. Therefore 1-D spatial signatures in the slice at this height are used to find where the femur is located. In these signatures the edge around the femur is located and the center of the femur are set to be in the middle of the area that is located in this way. This gives the x - and y -coordinates for the initial guess. See Figure 7.2 for illustrations of the location of the initial guess.

The rotation is assumed to be zero and thus no search is made to evaluate it. The reason for this assumption is that the coordinate system used is fixed to the body. If the knee is not straight problems can emerge because the bone will not point straight to the head.

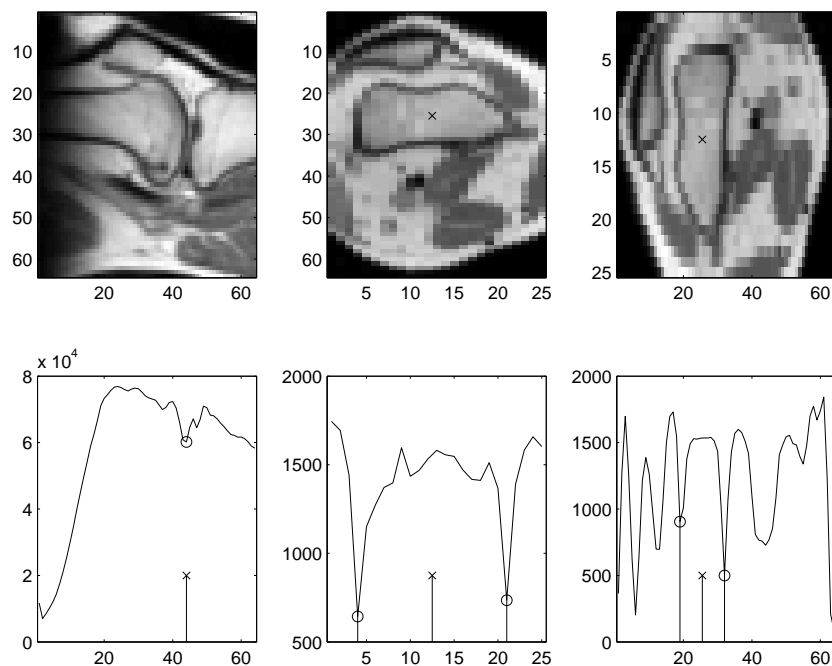


Figure 7.2: The 1-D spatial information of the 2-D images. To the left the sum of the columns is plotted, this sum is used to find the area between the femur and the tibia. The images in the middle shows how the x -coordinate is located. The two points marked with a circle are located and the x -coordinate is placed in the middle. To the right the location of the y -coordinate is located in the same way. The minimums located are those closest to column 25 in each direction. The location of the initial guess is marked with a \times in the image in the middle and in the image to the right.

7.3 Finding Suitable Points

To find the new point to place a landmark, while searching in the directions of the normal, mainly two approaches are possible. The easiest one is to look for the strongest edge. This approach however requires that the model points are placed at the strongest edge which is not always true. To handle this problem it is possible to build a model of the local structure near the landmarks in the training examples. A model for the mean appearance and the appearance variation along the surface normal at each landmark is built. And at the segmentation the best position is chosen for the landmark along the normal of the surface.

7.3.1 Modelling Local Structures

To model the variations of appearance for a specific landmark k sample points in the normal direction of the surface are evaluated, this gives $2k + 1$ equidistant points. These values usually have a big variation of intensity over the training set. To minimise this effect the derivative of the intensity is used. The sampled derivatives are put in a vector \mathbf{g}_i , the \mathbf{g}_i vector is in this thesis eleven elements long. These values are then normalised by dividing with the sum of absolute values of the vector,

$$\mathbf{g}_i \rightarrow \frac{1}{\sum_j |g_{ij}|} \mathbf{g}_i, \quad (7.1)$$

Figure 7.3 shows a typical profile for a landmark.

This is repeated for all surfaces in the training set and gives a set of samples $\{\mathbf{g}_i\}$ for each landmark. These are assumed to be Gaussian distributed and the mean $\bar{\mathbf{g}}$ and the covariance \mathbf{S}_g are calculated. This results in a statistical model of the grey level profile at each landmark.

Through the process from marking the interesting parts of the knee to building the triangulation with corresponding landmarks of the object small errors in the surface will probably be introduced. This will make the modelled surface to not be exactly suited to the real surface. Thus the profiles will be translated a bit and the benefit of model will be small. To reduce these problems an edge detection in a short distance along the normal to the surface is performed. If the edge detection finds a suitable edge the landmarks are moved to that position. The difference between this approach and a plain edge detection is that this only allows small movements from the landmark and if there are several edges and the edge looked for is not the strongest this make it possible to find a weaker edge next to the strong one.

The edge detection is made by fitting cubic splines to the sampled values in the profile. With aid of the new points that are calculated the edge can be located between the samples. The edge detection looks for places were the second derivative is zero. If those points also has a minimum in the first derivative the point is considered as an edge. The detection is made in two steps. First it is done in a coarse level and in a second step the detection is made in the level with the highest resolution.

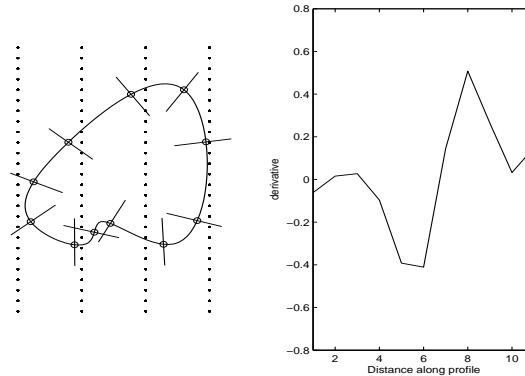


Figure 7.3: At each model point the derivative of the intensity are sampled along the normal direction. The dots in the left image shows where image data are located, between these slices interpolation is needed. To the right is a typical example of a boundary profile.

7.3.2 Getting New Points

When a new point is to be located, while searching in the direction of the normal during segmentation, the quality of the fit is measured by the Mahalanobis distances given by

$$f(\mathbf{g}_s) = (\mathbf{g}_s - \bar{\mathbf{g}})^T \mathbf{S}_g^{-1} (\mathbf{g}_s - \bar{\mathbf{g}}), \quad (7.2)$$

where \mathbf{g}_s is the sample made around the new point candidate. This value is linearly related to the probability that \mathbf{g}_s is drawn from the model. Thus minimising \mathbf{g}_s is the same as maximising the probability that \mathbf{g}_s comes from the distribution and therefore that the point is at the sought-after edge.

To find the suitable point $m > k$ values are sampled around the old place for the landmark and the new point is placed to best fit the profiles of the training set as described above.

7.3.3 Getting New Points in a Multi-Resolution Approach

The sampling of the gray level profiles for modelling the appearance is done in every level so that the fitting can be done in every scale. The length of the profile expressed in voxels is constant over the levels. This makes the length expressed in millimeters to search longer in the picture with the lowest resolution. In the coarse level only a few of the shape modes are used in the model. This helps the segmentation to not get stuck in a false edge.

To speed up the algorithm only a few of the landmarks are used in the coarse levels. In this thesis 1/4 of the landmarks are kept for every step to a coarser level.

7.4 Updating Parameters

When new landmark positions are located the next step is to update the parameters for translation, scale, rotation and shape modes to best fit the new points. This is done by an iterative process. The aim is to minimise

$$\|\mathbf{Y} - T_{t,s,\theta}(\bar{\mathbf{x}} + \Phi\mathbf{b})\|^2, \quad (7.3)$$

where \mathbf{Y} is the new points and T is a similarity transformation. The iterative approach is as follows:

1. Set the shape parameters \mathbf{b} initially to zero.
2. Generate the shape given by the present \mathbf{b} (See (6.8)).
3. Find the similarity transform that best fits the shape to the new points (See Chapter 5).
4. Calculate new parameters for \mathbf{b} according to (7.4).
5. Apply constraints on \mathbf{b} .
6. Return to step 2 until converged.

Since the shape modes are orthogonal it is easy to calculate the best parameters of the \mathbf{b} vector. If a shape $\tilde{\mathbf{x}}$ is the approximated shape to \mathbf{x} as $\tilde{\mathbf{x}} = \bar{\mathbf{x}} + \Phi\mathbf{b}$, the \mathbf{b} parameters can be calculated by multiplying by Φ^T which gives the result

$$\mathbf{b} = \Phi^T(\tilde{\mathbf{x}} - \bar{\mathbf{x}}). \quad (7.4)$$

In the segmentation only shapes relatively similar to the shapes in the training set is of interested. Therefore constraints are applied to the \mathbf{b} parameters. Usually those constraints are $\pm 3\sqrt{\sigma_i}$ where σ_i is the eigenvalue corresponding to shape mode i .

Chapter 8

Experiments

The difference between the two data sets on which the algorithms have been tested were primarily the resolution. In the MR images the resolution was about 0.5 mm in the slices and 3 mm between the slices, in the SPECT images the resolution was about 2 mm in all directions. In other words were the voxels cubic in the SPECT images and highly non cubic in the MR images.

8.1 Shape Reconstruction from Point Cloud

In the shape reconstruction the distance function was represented with a volume with 64 elements in each direction. With a larger volume a more detailed surface would be achieved but if the volume was doubled the fast marching algorithm was too time consuming. On the other hand the time for the algorithm only depending significantly on the volume size and not for example the number of points on the surface. The resulting surface looked well suited to the points, but no exact measurement has been done. The difference in the results for the MR images of the knee and the SPECT images of the brain was primarily connected to the density of points in the point cloud representing the surface. In the MR images the marking was done in at least sagittal and coronal images and therefore there was no big open areas in the point cloud. On the SPECT images marking of the brain was only done in transversal slices and because of that a big open area was left in the top of the brain (Figure 3.2). The result of the open area was a concave top of the brain that was false. To fix that problem new points were interpolated at the top of the point cloud. Another approach should be to mark the brain in a second direction.

8.2 Finding Corresponding Points

The result of the ICP algorithm of the knee surfaces was not satisfying when corresponding points were to be found between a right and a left knee, even if the knees looked almost the same visually. Therefore the left knees were mirrored in the x -direction. After that there was no significant difference between the result of a left and a right knee.

A source to make the result worse was that the images did not cover exactly the same area in the top. That made the surfaces sometimes cover a larger part

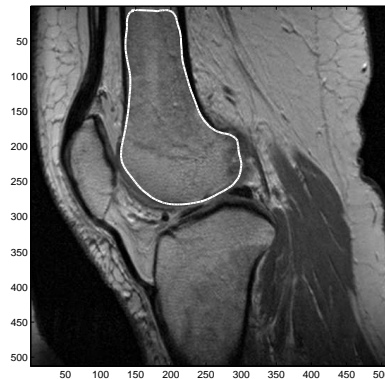


Figure 8.1: A good result from the segmentation when only plain edge detection have been used while updating landmark positions.

of the femur in the knee images and in the brain images the whole brain was not always covered. This means that there are no true corresponding point on the surfaces. Because of this it arise strange artifacts on the top of the femur on some shapes.

8.3 Segmentation

The result of the segmentation showed big difference between the MR images and the SPECT images. The result was significantly better on the SPECT images.

8.3.1 Results for MR Images of the Knee

The segmentation of the femur was difficult. There were mainly two problems; finding the initial guess and taking benefit of the modelling of the local gray level structure.

When the initial guess was not good enough the model was not able to find the way to the femur. Instead other edges were located that were of no interest (often the edge of the volume).

Without searching for edges in the building of the profiles, the model for the local structure was of no use. This made the segmentation algorithm to only find the object in a few pictures in this case. Then it was a better approach to just make an edge detection when updating landmark positions without any use of prior knowledge of the appearance. But in this case the result is not always the right edge. In Figure 8.1 the result is good and the right edge is detected. But in Figure 8.2 the wrong edge had been detected in the lower part of the knee.

When the improved models of the edges were used the result was significantly better. If the initial guess was good enough the search algorithm found the right edges almost every time. But in some parts of the images the result was not as good. During the segmentation only the sagittal images were used and if the result were visually examined the result looked better in the sagittal view. In Figure 8.3 the result from a segmentation is viewed.

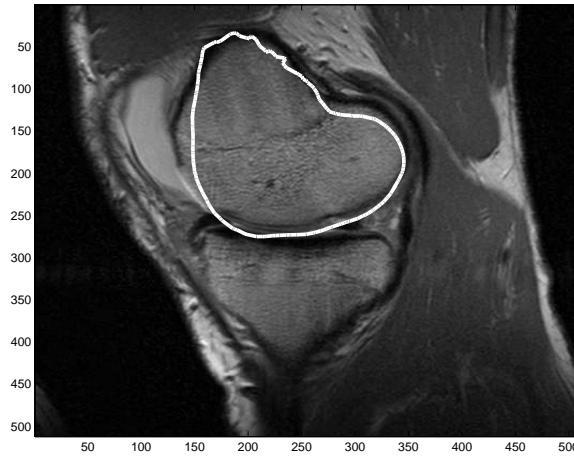


Figure 8.2: A bad result from the segmentation when only plain edge detection have been used while updating landmarks positions.

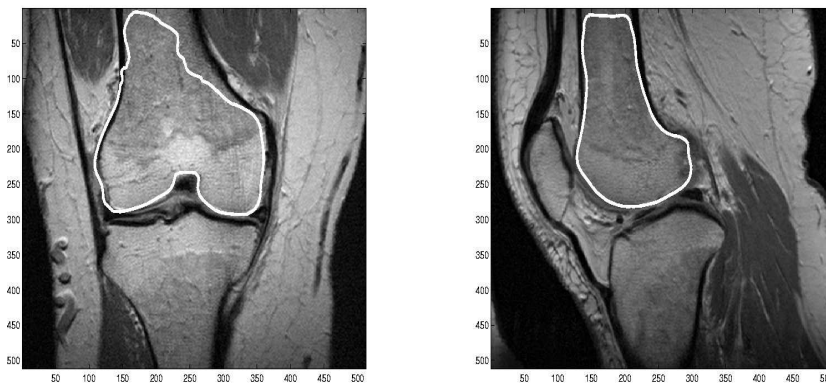


Figure 8.3: The result of the segmentation when the model of the gray level structure were used. The segmentation was applied in sagittal images and the result looks better in the sagittal view. (The sagittal slice is the same as in Figure 8.1.)

8.3.2 Results for SPECT Images of the Brain

When the segmentation was done on the SPECT images a better result was obtained. When the algorithm was used on a number of brains and the result was compared to the points marked on the surface it was hard to tell which were the choice of the computer and which were chosen by the expert.

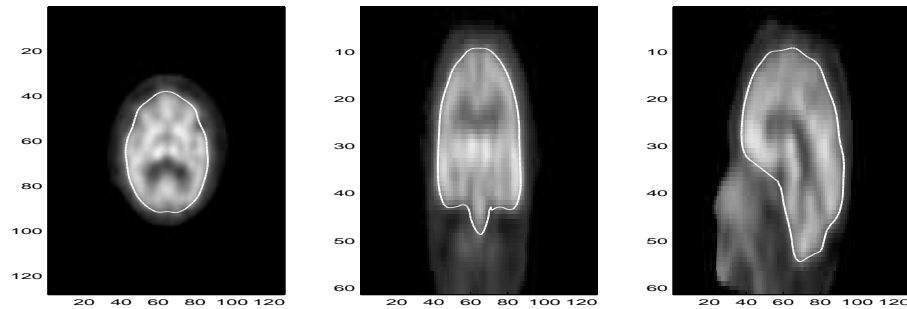


Figure 8.4: The result of the segmentation on SPECT images of the brain.

8.3.3 Difference Between the Result of SPECT and MR Images

There can be several reasons why the result was better with the SPECT images of the brain than the MR images of the knee. The most obvious is that the initial guess was better in the SPECT images where almost the only visible thing was the brain, even if there were some structures for example in the neck that were also visible. In the knee images the muscles and the fat around the femur are also visible which makes it a harder task to find a good initial guess.

A big difference between the images was the shape of the voxels. In the SPECT images the voxels were cubic. But in the MR images one dimension was ten times larger than the others. This is probably a major drawback for example when the local structures are modeled. When the correspondence across the training set is not perfect there is a large risk that one normal that points in a direction parallel to the image slice in one training example points more orthogonal to the slice in another example. When the normal points parallel to the slice a high amount of variation can be measured but when it points orthogonal to the slices almost no variation can be measured. The problem with the knee images often appears on a more detailed level when the voxels are less cubic, while the segmentation works better on a coarse level where the voxels are almost cubic.

Chapter 9

Further Work

The thesis is divided in the parts shape reconstruction, model building and segmentation. The first part is the one where least further work is necessary, even if it would be desirable that the surface reconstruction worked on a more sparse point cloud.

9.1 Improvements on the Model Building

For the model building the improvement lies in finding the corresponding points between the shapes in the training set. A commonly used method to measure how well points correspond over the training sets is to calculate the description length (DL). This method is used in many different fields. The concept of minimum description length (MDL) comes from information theory. The aim is to minimise the amount of information needed for a full description of the training set. The idea is that by minimising the description length it will be a trade-off between a simple model that thus is general and getting a model that well represents new shapes that is not in the training set. This approach should favour models that are well suited for describing new shapes which are similar to those in the training set and at the same time the model should badly describe those shapes that are not similar. Hopefully the shapes should be well described by a few number of modes.

The data is transmitted as a shape model as in (2.1). To transmit the whole training set the mean $\bar{\mathbf{x}}$ and the shape modes Φ need to be transmitted one time. Therefore the aim of the optimisation is to make the parameters in \mathbf{b} as small as possible over the training set.

Some work has been done by Karlsson [10] in optimising the MDL. The algorithms in that thesis was too time consuming to use for a more practical application as in this thesis. One of the reasons for this was that the algorithm for optimisation was global. It should be an interesting approach to shift the optimiser made by Karlsson to a local optimiser and give the result from the ICP algorithm as initial guess. For more about MDL see Ericsson [7].

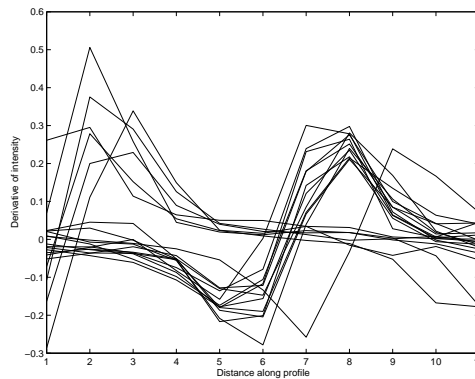


Figure 9.1: An example of a profile that has two different forms of gray level signature.

9.2 Further Work on Segmentation

The appearance models that are used for the edge detection assumes that the distributions are Gaussian. This assumption is not correct for all points, as can be seen in Figure 9.1. In that case two different gray level structures describes the edge in different images. Therefore it is necessary to change the searching for new points to an algorithm that can handle this sort of variations.

To overcome the problem that the result was better in the slice direction that was used for the segmentation, may be solved by making separate searches for new points in the different slice directions and then take the best location, in some meaning, for the new point.

Another way to improve the result is to take advantage of the multi-spectral images that are produced with MRI. For example the cartilage is bright in one type of the images. This should make it easier to find the right edge in the lower part of the femur and of course to segment the cartilage.

9.3 A New Approach for the Searching After New Points

When the search is made in the normal directions of the surface the information density can be low in the search direction (Figure 7.3). If instead the search was forced to be in the direction of the images, the information in the images might be more effectively used. But as can be seen in Figure 9.2 this implies new problems. Primarily two problems have to be solved.

The first problem is that the new edge to be located will not be placed in the same position on the surface over the iterations. This means that in every step the location of the point at the surface has to be located. This will lead to the model fitting process becoming a much harder task.

The other new problem is the modelling of the local structure near the boundary. If this approach for searching is used the points where to search moves over the iterations and the searching for new points is not made in a specific direction compared to the surface.

Bibliography

- [1] D. Adalsteinsson and J.A. Sethian. The fast construction of extension velocities in level set methods. *Journal of Computational Physics*, 148:2–22, 1999.
- [2] National Electrical Manufacturers Association. Digital imaging and communications in medicine. <http://medical.nema.org/dicom/2004.html>, 2004.
- [3] P.J. Besl and H.D. McKay. A method for registration of 3-d shapes. *Pattern Analysis and Machine Intelligence, IEEE Transactions on*, 14:239–256, 1992.
- [4] P.M.M. Cashman, R.I. Kitney, M.A. Gariba, and M.E. Carter. Automated techniques for visualization and mapping of articular cartilage in mr images of the osteoarthritic knee: a base technique for the assessment of micro-damage and submicro damage. *Nanobioscience, IEEE Transactions on*, 1(1):42–51, 2002.
- [5] Z.A. Cohen, D.M. McCarthy, S.D. Kwak, P. Legrand, F. Fogarasi, E.J. Ciaccio, and G.A. Ateshian. Knee cartilage topography, thickness, and contact areas from mri: in-vitro calibration and in-vivo measurements. *Osteoarthritis and cartilages*, 7:95–109, 1999.
- [6] T.F. Cootes and C.J. Taylor. Statistical models of appearance for computer vision. http://www.isbe.man.ac.uk/~bim/Models/app_models.pdf, 2004.
- [7] A Ericsson. Automatic shape modelling and applications in medical imaging. Licentiate thesis, Dept. of Mathematics, Lund Institute of Technology, Sweden, 2003.
- [8] S. Ghosh, O. Beuf, M. Ries, N.E. Lane, L.S. Steinbach, T.M. Link, and S. Majumdar. Watershed segmentation of high resolution magnetic resonance images of articular cartilage of the knee. In *Engineering in Medicine and Biology Society, 2000. Proceedings of the 22nd Annual International Conference of the IEEE*, volume 4, pages 3174–3176, 2000.
- [9] V. Grau, A.U.J. Mewes, M. Alcaniz, R. Kikinis, and S.K. Warfield. Improved watershed transform for medical image segmentation using prior information. *Medical Imaging, IEEE Transactions on*, 23(4):447–458, 2004.
- [10] J. Karlsson. Automatic positioning of landmarks for shape analysis. Master’s thesis, Dept. of Mathematics, Lund Institute of Technology, Sweden, 2002.

-
- [11] Dzung L. Pham, Chenyang Xu, and Jerry L. Prince. Current methods in medical image segmentation. *Annual Review of Biomedical Engineering*, 2:315–337, 2000.
- [12] Yonggang Shi and W.C. Karl. Shape reconstruction from unorganized points with a data-driven level set method. In *Acoustics, Speech, and Signal Processing, 2004. Proceedings. (ICASSP '04). IEEE International Conference on*, volume 3, pages 13–16, 2004.
- [13] S Spanne. *Föreläsningar i matristeori*. KFS i Lund AB.
- [14] T. Stammberger, F Eckstein, M Michaelis, K.H. Englmeier, and M Reiser. Interobserver reproducibility of quantitative cartilage measurements: comparison of b-splines snakes and manual segmentation. *Magnetic Resonance Imaging*, 17(7):1033–1042, 1999.
- [15] S Svanberg. *Multi-Spectral Imaging, from astronomy to microscopy, from radiowaves to gammarays*. KFS i Lund AB, 2003.
- [16] J.G. Tamez-Pena, K.J. Parker, and S. Totterman. The integration of automatic segmentation and motion tracking for 4d reconstruction and visualization of musculoskeletal structures. *Biomedical Image Analysis, 1998. Proceedings. Workshop on*, pages 154–163, 1998.
- [17] S. Umeyama. Least-squares estimation of transformation parameters between two point patterns. *Pattern Analysis and Machine Intelligence, IEEE Transactions on*, 13:376–380, 91.
- [18] H.-K. Zhao, S. Osher, B. Merriman, and M. Kang. Implicit and nonparametric shape reconstruction from unorganized data using a variational level set method. *Computer Vision and Image Understanding*, 80:295–314, 2000.
- [19] H.-K. Zhao, Chan T., B. Merriman, and S. Osher. A variational level set approach to multiphase motion. *Journal of Computational Physics*, 127:179–195, 1996.